The International Journal of Advanced Manufacturing Technology (2020) 106:371–383
https://doi.org/10.1007/s00170-019-04641-x

ORIGINAL ARTICLE

Effects of powders and process parameters on density and hardness of A357 aluminum alloy fabricated by selective laser melting

Lavinia Tonelli[1] · Erica Liverani[2] · Giuseppe Valli[1] · Alessandro Fortunato[1] · Lorella Ceschini[3]

Received: 10 August 2019 / Accepted: 4 November 2019 / Published online: 21 November 2019

Abstract

Additive manufacturing processes based on the local fusion of a powder bed, such as selective laser melting (SLM), are a valid alternative to conventional technologies and a growing number of industrial sectors are currently relying on these processes for the production of different components. However, there are still some limits in using SLM and they are often related to the feedstock material. For this reason, in the present work, the effects of powder properties and pre-treatments, as well as process parameters, on the fabrication of aluminum alloy A357 samples were investigated. Two different batches of powder were considered in order to evaluate the effects of particles shape and size in the as-received condition and after two different pre-treatments: 60 °C for 3 h and 200 °C for 1 h. Selective laser-melted samples were produced in the conditions described above and were then characterized in terms of density, phase and chemical composition, defects, and hardness. The results showed a correlation between powder conditions in terms of morphology and pre-treatment on the properties of SLM A357 aluminum alloy components.

Keywords Aluminum alloy · Selective laser melting · Pre-treatment · Powder feedstock · Additive manufacturing

1 Introduction

Currently, selective laser melting (SLM) is the most used metal powder bed additive process since it is a valid solution for the production of various and different components. A growing number of research groups are working on the development and the optimization of SLM and the literature shows vast opportunities to exploit the potential of this process. Several works addressed the problem of optimizing process parameters, both from a technological [1–3] and a metallurgical [4–6] point of view. These papers demonstrated that it is possible to reach near-full densities and good mechanical properties using SLM. Furthermore, the research topics concerning aspects related to residual stresses [7, 8] and the need of post-processes [9–11] have proposed several useful solutions.

Many of the outcomes mentioned above are probably linked to the feedstock. The presence of porosity in SLM builds, in fact, is not always caused by un-optimized process parameters, but can also be related to the presence of porosities in the initial batch of powder due to trapped atomization gas [12]. Moreover, pores in SLM components can result from non-spherical geometry and from the presence of attached "satellites" on main powder grains that compromise the packing capacity of the powder bed and prevent the correct deposition of the layer [13]. Powder properties such as flowability and packing density are also influenced by the particle size distribution and both are strictly related to the final properties of SLM production. Several authors have demonstrated that powder has to achieve good random close packing; therefore, a mixture of both large and small particles is needed, since the presence of fine particles allows filling the voids between the

Electronic supplementary material The online version of this article (https://doi.org/10.1007/s00170-019-04641-x) contains supplementary material, which is available to authorized users.

✉ Lavinia Tonelli
lavinia.tonelli2@unibo.it; lavinia.tonelli@gmail.com

[1] Department of Industrial Engineering (DIN), Alma Mater Studiorum - University of Bologna, Viale Risorgimento 2, 40136 Bologna, Italy

[2] Interdepartmental Center for Industrial Research - Advanced Applications in Mechanical Engineering and Materials Technology (CIRI - MAM), Alma Mater Studiorum - University of Bologna, Bologna, Italy

[3] Department of Civil, Chemical, Environmental and Materials Engineering (DICAM), Alma Mater Studiorum - University of Bologna, Bologna, Italy

coarser ones [14–16]. Nevertheless, if the particle size distribution is too wide, the laser power is unable to melt the largest particles or might over-melt the small ones, leading to unmelted regions, spatter, and balling effects [17]. Furthermore, particles finer than ~ 10 μm favor cohesion, thus increasing powder agglomeration, and consequently decrease the flowability, resulting in a non-uniform powder bed [18, 19]. Moreover, the surface of aluminum powders reacts with oxygen to form a passivation aluminum oxide layer that absorbs humidity. A large number of fine particles increase the surface area in contact with air and thus the amount of adsorbed water, which compromises the powder flow [20]. According to Herbert [21], the metallurgy of powder bed fusion technologies is strongly influenced by the feedstock quality: water absorption, formation of oxides, and hydroxides layers can negatively affect not only the powder flowability but also the melting and solidification processes. In case of oxide layer covering powder particles, for example, most of the laser beam heating is absorbed by the layer, since it requires high temperature to undergo melting. In addition, due to the low specific heat capacity of oxides, also heat conduction is reduced. Furthermore, water absorption can be detrimental for flowability of the powders, thus compromising the proper spreading of particles, but it may also lead to changes in the chemical composition, as a consequence of the hydrogen dissociation [21, 22]. So, powder pre-treatments and proper storage solutions have to be considered.

Many of the considerations above can be extended also to the recycled powder, but in that case, the experiments led to different results. It is well known that over-heated powders increase dimensions and change their morphology and rheology behavior. However, some authors have shown that sieving allows to separate these grains from the others and to obtain a recycled powder very similar to the initial feedstock [23], while other papers stated the opposite [24].

The state of art gives a wide overview of the rheological properties of powder affecting the SLM process for several alloys regularly used. However, these data are not yet sufficient to completely understand the effects of the raw material on the final properties of the components [22]. The main reason is that powders are strongly influenced by the storage and handling conditions and they are not always maintained in a controlled humidity and temperature environment. Therefore, the storage condition must be examined and possible solutions to re-establish the as-received properties of powders must be carried out. In particular, aluminum alloys can easily react with air oxygen and aluminum powders are strongly influenced by the presence of humidity. For the authors' knowledge, Li et al. in [25] were the first to deal with these aspects, but considering only one initial condition, both in terms of type of powder and the possible thermal treatment to perform before process. In a recent work, Muñiz-Lerma et al. [20] performed a comprehensive characterization of A356 and A357 powders for additive manufacturing (AM) subjected to a 200 °C pre-treatment, and they even propose interesting and non-traditional techniques to determine powder properties. However, they did not correlate the powder properties to the resulting samples.

In this work, the authors have chosen to enrich the knowledge about the effect of powder properties and pre-treatments, as well as process parameters, on the fabrication of aluminum SLM samples. In this view, two different virgin A357 powders were considered, nominally with the same chemical composition and supplied by the same manufacturer, but obtained with different processes. On both powders, the effect of two preliminary treatments that could eliminate the humidity effect due to an uncontrolled storage was evaluated. SLM samples were fabricated by using the two powders, subjected to the different pre-treatments, and by varying the process parameters, in order to correlate final properties of samples to both the process conditions and the quality of the powder feedstock. In particular, the authors have analyzed the mutual effects of the described factors as follows: (i) influence of pre-treatment on powder morphology; (ii) influence of powder morphology (axis major and aspect ratio) on samples' density and hardness; (iii) influence of pre-treatment temperature and soaking time on samples' density and hardness; (iv) influence of process parameters (laser power and scan speed) on final samples density, hardness, and defects.

2 Experimental procedure

In the present study, two different gas atomized powders of the A357 aluminum alloy (Aluminum Association designation [26]) were considered for the production of AM samples. Both powders were produced by the same supplier (LPW Carpenter Additive, Carpenter Technology Corporation, USA) adopting two different processes, whose details cannot be disclosed since they represent industrial sensitive information. Powders belonging to the two sets will be referred to as powder L and powder H hereafter. Basing on the data provided by the supplier, reported in Table 1 for chemical composition and Table 2 for other powder properties, they mainly differ in the Mg and N content, higher in powder H than powder L, and in powder properties, such as flowability and apparent density. The latter properties, in particular, were not provided for powder L since, in this case, particles tend not to flow at all.

2.1 Fabrication of SLM samples

A preliminary experimental campaign was carried out by producing samples with powders in the as-received condition; however, in the reason of the poor flowability ascribable to the high humidity content, results were unsatisfactory. So,

Table 1 Chemical composition (wt.%) of powders, given by the supplier [27]

	Al	Si	Mg	Fe	Cu	Mn	Ti	Zn	O	N	Other
Powder L	Bal.	6.96	0.49	0.10	0.01	< 0.01	0.09	< 0.01	0.1	< 0.001	< 0.15
Powder H	Bal.	6.90	0.55	0.09	< 0.05	< 0.01	0.09	< 0.01	0.1	< 0.2	< 0.1

both powders H and L were subjected to a drying pre-treatment, with the aim to reduce the adsorbed humidity. Two kinds of heat treatments were investigated: a high-temperature drying and a low-temperature one. The first heat treatment consisted of heating the powder up to 60 °C and soaking for 3 h, the second one of heating up to 200 °C and soaking for 1 h.

In both cases, the heat treatment was carried out in a muffle furnace, in ambient atmosphere, using a heating ramp of 100 °C/h and an air cooling.

All samples were built in a SLM machine (MYSINT100 RM manufactured by SISMA) equipped with a 200 W fiber laser source with a spot diameter of 55 μm. Melting process was carried out in a nitrogen environment with a residual oxygen content of 0.1 vol.%.

Process parameters, like building orientation, supports generation, laser power, scanning velocity, and strategy, were defined using the Autofab software by Materialise.

A roto-translating 3 × 3 mm^2 chessboard was used for scanning the bulk volume of each sample. The distance between laser tracks (hatch distance) inside the chessboard was fixed at 70 μm and the layer thickness was set at 20 μm. Building direction was chosen as vertical and the samples (with dimensions 10 × 10 × 15 mm^3) were randomly distributed in the building plate. In order to compare the two different types of powders and the two different powder pre-treatments, a total of four set of samples were realized with the process parameters shown in Table 3.

2.2 Powders characterization

Free surfaces and cross-sections of the powders were analyzed in the as-received condition and after pre-treatment (soaking at 200 °C for 1 h and at 60 °C for 3 h) by means of scanning electron microscopy with energy dispersive X-ray spectroscopy (SEM-EDS, Zeiss EVO 50). Particles characterization, in terms of size distribution and aspect ratio, was carried out on SEM micrographs of free powders via image analysis, using the ImageJ open source software [28]. X-ray diffraction (XRD, PANalytical Expert PRO with Xcelerator detector) was used to determine phase composition of the powders, both as-received and heat-treated. A Cu-Kα radiation source (λ = 0.15406 nm) was adopted and θ–2θ scans were carried out from 20 to 140°, with a 0.017° step size and a 25 s dwell time, operating at 40 kV and 40 mA.

2.3 SLM samples characterization

Density of the SLM samples was measured with an analytical balance (0.0001 g precision), by adopting the Archimedes principle. Hardness was evaluated by performing HBW 2.5/62.5 Brinell measurements, hence referred to as HB10 where 10 stands for the force/diameter ratio, as reported in the ASTM E10-18 standard. For all samples, the hardness was measured in the as-built condition, within 12 h from the end of the process. Topography of top surfaces was characterized by means of 3D-digital microscopy (Hirox KH-7700). Chemical composition of the SLM samples was determined by Glow Discharge Optical Emission Spectroscopy (GDOES, GDA-650 Spectrum Analytik GmbH), while phase composition was evaluated by XRD, under the same operating conditions used for the powders and already described in Section 2.2.

For metallographic analyses, cross-sections were extracted from the SLM samples considering both longitudinal and transverse directions, with respect to the building one. Subsequently, the cross-sections were prepared for the microstructural characterization following standard metallographic procedures and chemically etched with Keller's reagent (20 s immersion at room temperature) [29]. Metallographic specimens were observed by means of an optical microscope (OM, Zeiss Imager A1) and by SEM-EDS; then, porosity measurements and defects characterization were performed using the ImageJ software.

Table 2 Powder properties, given by the supplier [27]

	Laser size diffraction (μm) (ASTM B822)			Sieve analysis (wt.%)	Carney flow (s/75 g) (ASTM B213)	Apparent density (g/cm^3) (ASTM B212)
	DV(10)	DV(50)	DV(90)	+ 63 μm	–	–
Powder L	19.8	40.4	73.2	0	–	–
Powder H	26.0	40.0	62.0	0	38.25	1.3

Table 3 Process parameters adopted for the fabrication of SLM samples

Laser power (W)	Scan velocity (mm/s)	Energy density (J/mm^3)
70	500; 700; 900; 1200	100–41.7
90	500; 700; 900; 1200	128.6–53.6
110	500; 700; 900; 1200	157.1–65.5
130	500; 700; 900; 1200	185.7–77.4
150	500; 700; 900; 1200	214.3–89.3
170	500; 700; 900; 1200	242.9–101.2

3 Results and discussion

3.1 Powders quality

Representative SEM micrographs of L and H free powders and powders' cross-section, in the as-received condition, are reported in Fig. 1. Particles of powder H were generally more spherical than those of powder L, where elongated particles were more present. In the case of powder H, several small and almost perfectly spherical particles can be found; the same does not apply to powder L. As shown in Fig. 1 (a) and (b), the surface morphology of both set of powders was irregular, since numerous satellites and collapsed particles can be recognized on the surfaces. The analysis of powders' cross-section, reported in Fig. 1 (c) and (d), showed that they were characterized by a dendritic phase (as highlighted by the optical micrograph in the inset) and they were mainly defect-free, even if in few cases typical solidification defects such as gas porosities, interdendritic shrinkages, and possibly bi-film oxides were detected [30]. As for the latter, semi-quantitative chemical analyses obtained by means of SEM-EDS are reported in Fig. 2, revealing a higher content of Si and O in correspondence of such defects (spectra 1 and 2), with respect to the A357 alloy (spectrum 3).

Size and shape of the powder particles were measured via image analysis on SEM micrographs of free particles both in the as-received and pre-treated conditions (200 °C for 1 h and 60 °C for 3 h). Results, in terms of major axis and aspect ratio of the particles, are reported in Fig. 3. These two parameters were chosen to characterize the powders since major axis quantifies the maximum dimension while the aspect ratio determines the roundness of the particles, being the ratio between the major and the minor axis. The size distribution of both powders L and H, ranging from 5 to 80 μm, is asymmetric and a positive skewness can be recognized, meaning that the size of the majority of particles lies at low values. In particular, in the as-received condition almost 40% of powders L and H had an axis major below 25 μm. Moreover, if only small powders with a size of up to 10 μm are considered, the percentage is 8.5 for powder L and 30.8 for powder H, showing that the latter had a consistent amount of small particles. This data confirms that an irregular shape of powder grains increases cohesive forces between particles [31].

The percentage of particles with dimensions greater than 45 μm was, however, similar for both powders, being 13.1 for powder L and 12.4 for powder H. By comparing the results obtained by image analysis and the ones given by the supplier and retrieved by laser diffraction (Table 2), it appears that the analysis performed via laser diffraction slightly overestimated the size of powder particles.

Furthermore, Fig. 3 shows that, after the pre-treatment, the percentage of small particles (with major axis less than 15 μm) is lower than in the as-received condition, in particular for powder H. The result is confirmed also by SEM images

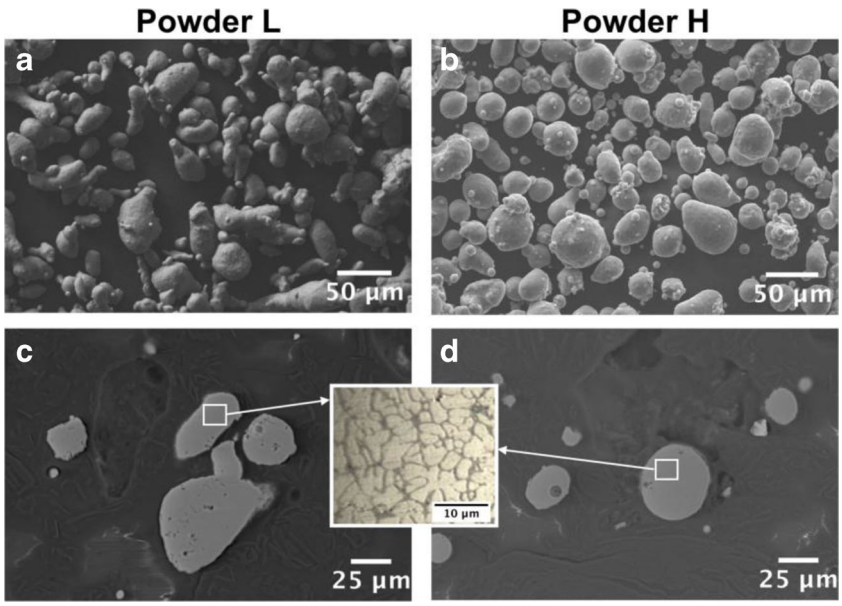

Fig. 1 Representative SEM images of as-received powders. (a, c) Free powders and powders cross-sections for powder L. (b,d) Free powders and powders cross-sections for powder H. In the inset, an optical micrograph showing dendritic phase of powders

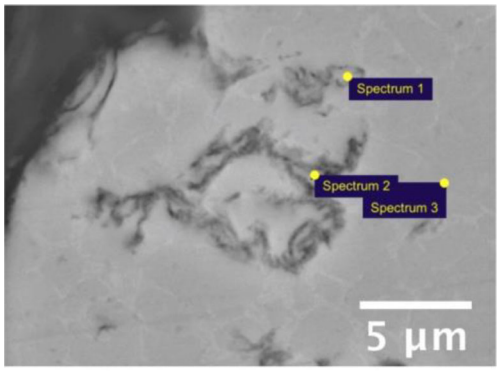

Element (wt.%)	Al	Si	Mg	O
Spectrum 1	88.53	9.90	0.34	1.23
Spectrum 2	84.98	11.2	0.28	3.52
Spectrum 3	95.65	3.42	0.28	0.62

Fig. 2 Results of SEM-EDS analysis performed on powder cross-section

reported in Fig. 4. The apparent loss of small particles can be explained in the reason of the cohesion forces action [18, 19, 32]. For small particles, indeed, the cohesive forces are able to agglomerate powders and this phenomenon is accentuated if the temperature rises. When the particle size increases, the ratio between the weight of a single particle and the cohesive force acting on it increases, making the forces unable to stabilize the cohesion between powder grains.

In addition, image analysis demonstrated that particles belonging to powder H are significantly more spherical than those to powder L: 31.8% of particles of powder H exhibited an aspect ratio from 1 to 1.1, thus almost perfectly spherical, with respect to 5.4% for powder L. By focusing on particles with the aspect ratio of up to 1.5, the percentage raises up to 77.3 for powder H and only 47.4 in case of powder L. In addition, it is worth mentioning that a non-negligible number of powder L particles, 4.7% of the total, had an aspect ratio greater than 3, meaning that almost 5% of powder L was made of strongly elongated particles. Pre-heating treatments seem not to have affected the shape of powders, since only small differences occurred in the measurements, ascribable to experimental variance.

In Fig. 5, XRD spectra of both powders L and H, in the as-received and heat-treated conditions, are compared. Al is the main phase detected (ICDD: 4-0787), but also minor peaks of silicon (ICDD: 27-1402) and alumina can be recognized. In

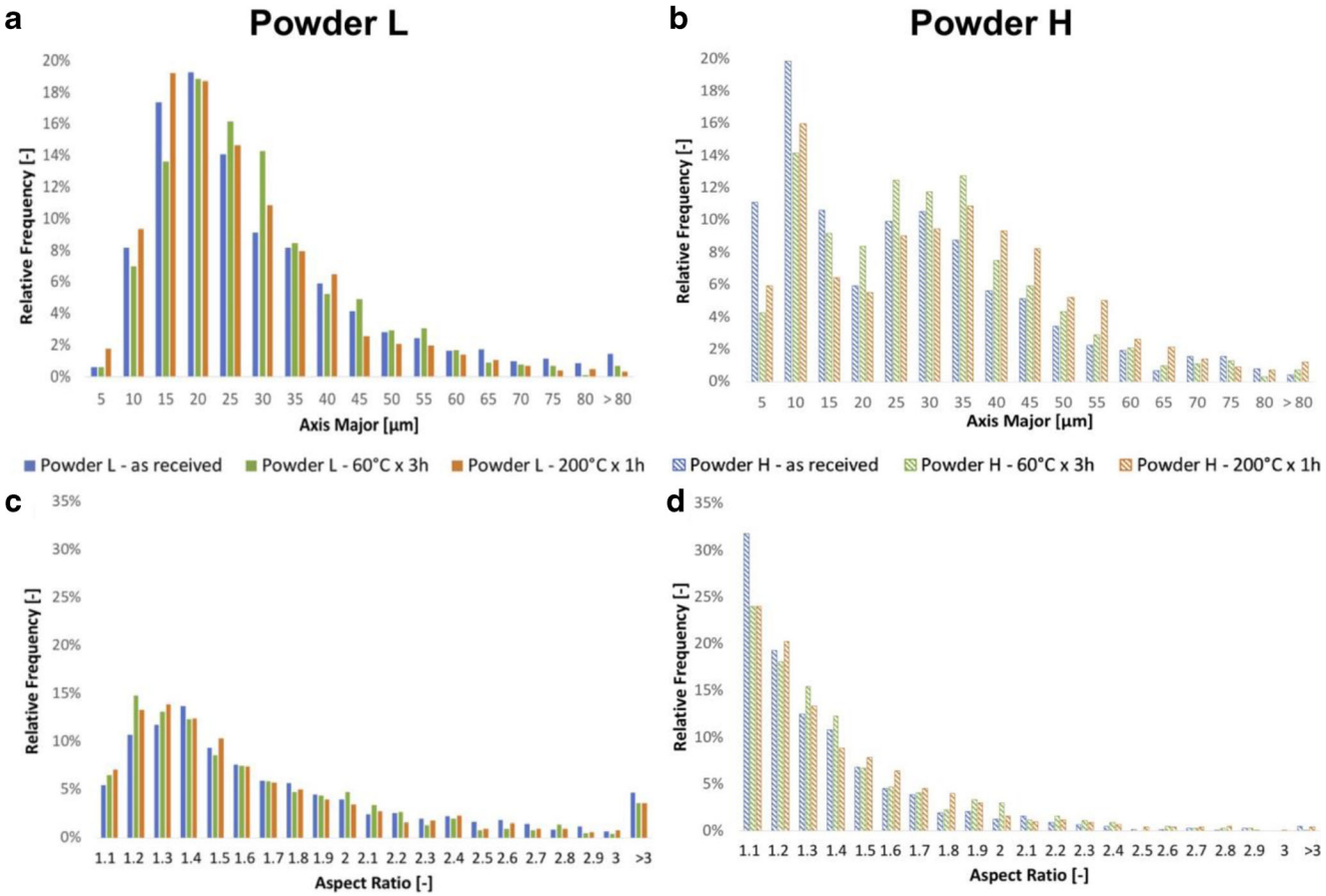

Fig. 3 Results of particles analysis. (a, c) Axis major and aspect ratio for powder L. (b, d) Axis major and aspect ratio for powder H

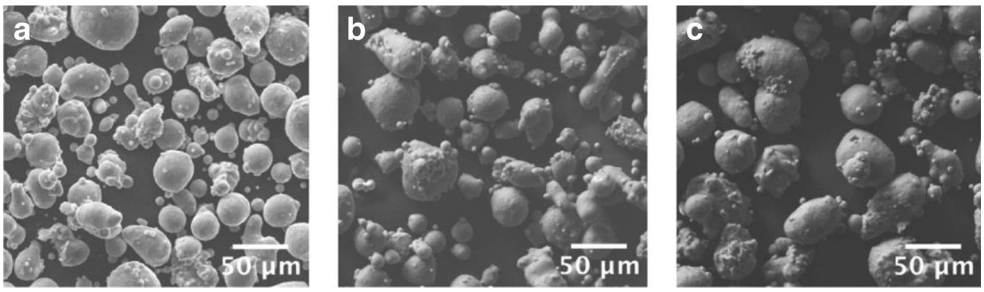

Fig. 4 Representative SEM images of powders in (a) as-received condition, (b) after a 60 °C pre-heating, and (c) after a 200 °C pre-heating

particular, the peak located at 25.4° is consistent with α-Al_2O_3 phase (ICDD: 46-1212) [33]. By focusing on the range between 20 and 30° (Fig. 5(b)), it is possible to appreciate that the α-Al_2O_3 was detected neither in powder L nor H after the treatment at 60 °C for 3 h, while it was found in the as-received powder and also after the treatment at 200 °C for 1 h. Superficial oxidation is a known issue that concerns AM powders. In a recent study carried out on different materials [34], XPS analyses showed the presence of a thin layer of oxide on the surface of powders in the as-received condition, even if produced with advanced technologies such as VIGA and plasma atomization.

Given the tendency of aluminum to react with oxygen and to form aluminum oxide, as well as the high surface-to-

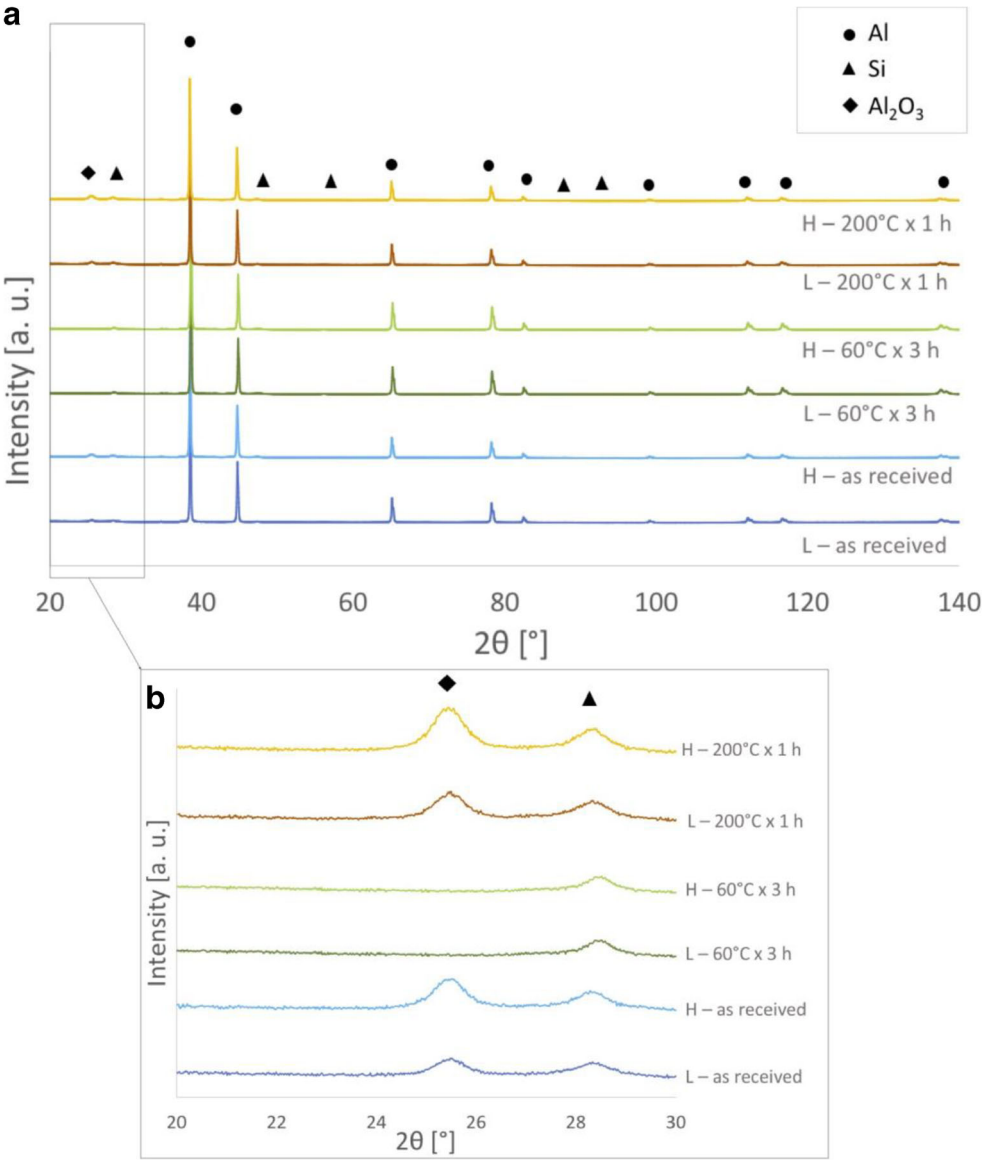

Fig. 5 XRD patterns for both powders L and H in the as-received and pre-treated conditions. (a) General view of the whole spectra. (b) Detail of the range $20° < 2\theta < 30°$

Table 4 Ratio between the areas of Al [111] and Al_2O_3 [012] peaks resulting from XRD analyses, for powders L and H in the as-received condition and after 200 °C for 1 h treatment

Powder	Condition	Al_2O_3/Al
L	As-received	0.031
H	As-received	0.038
L	200 °C × 1 h	0.037
H	200 °C × 1 h	0.058

volume ratio in the case of micron-sized powders, it is reasonable that aluminum oxide was detected by XRD analyses. After the heat treatment at 60 °C for 3 h, the peak of α-Al_2O_3 phase disappeared: it can be argued that the brittle alumina surface layer experienced thermal shock and developed cracks during the heat treatment, due to tensile stresses induced by the thermal expansion of aluminum powders. The α-Al_2O_3 phase was observed again after the heat treatment at 200 °C: it is possible that aluminum oxide still experienced thermal shock but the high temperature promoted the formation of a new oxide layer. In fact, by comparing the integrated diffraction intensity of the Al [111] peak located at 38.5° and the one of α-Al_2O_3 [012] peak located at 25.4° (Table 4), it can be argued that after the heat treatment, aluminum oxide phase raised for both powders, and the increase was more consistent in the case of powder H.

3.2 Effect of SLM parameters

In Fig. 6, the density of SLM samples, as a function of laser power, is reported. In order to compare all results, in the same plot, both data of samples produced with powder pre-heated at 60 °C and 200 °C are displayed. Density of samples strictly depends on laser power: for powder H, the relation between power and density was almost linear and, by increasing the power, the density of SLM samples increased accordingly. Powder L, instead, presented a threshold value of 110 W, since only in case of laser power beyond 110 W, the density increased linearly with the power. It is well known that one of the major complications of processing aluminum with SLM is the formation of thin oxide layer on the free surface of the melt pool, even if the process is carried out in an inert atmosphere

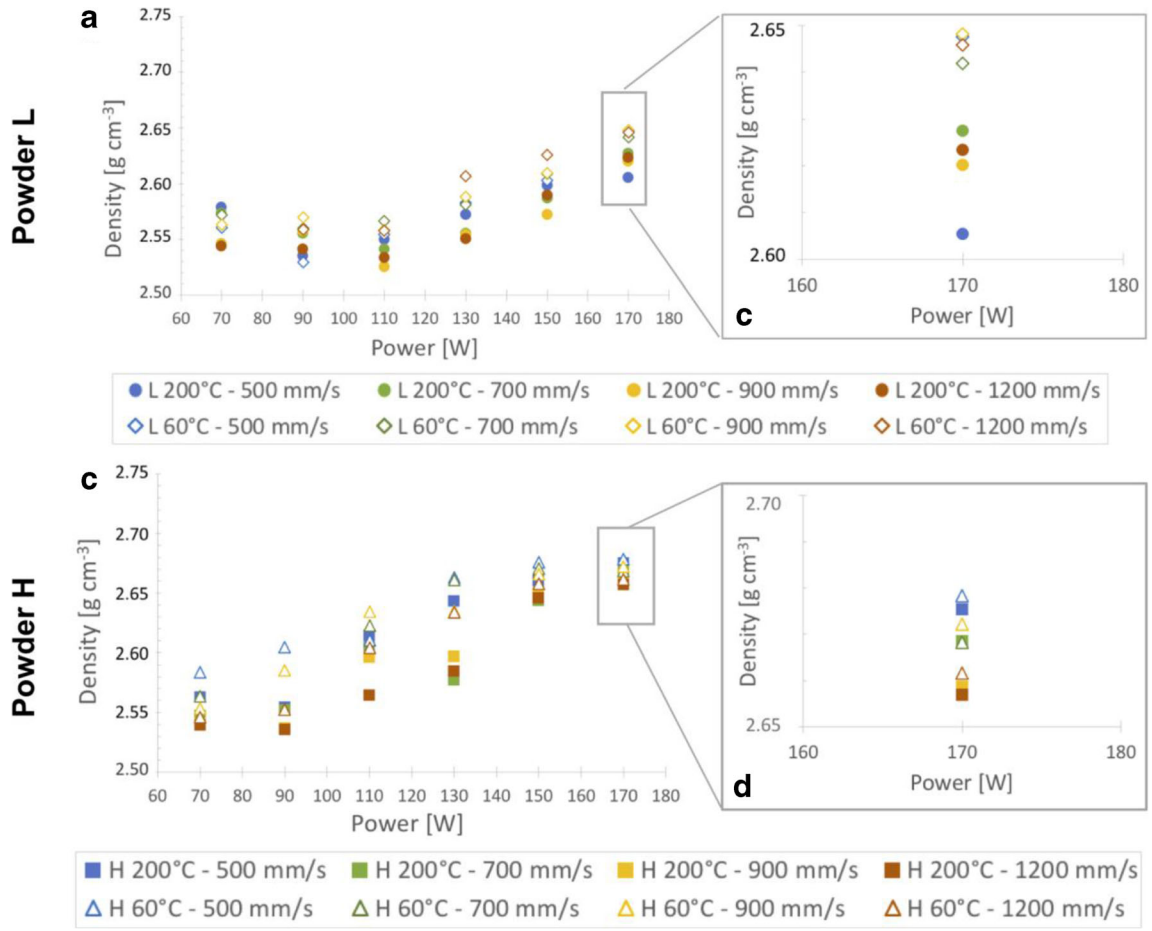

Fig. 6 Results of density measurements as a function of laser power and scanning velocities. (a) Samples produced with powder L. (c) Samples produced with powder H. (b, d) Details on samples produced with higher power for powders L and H, respectively. Numerical data are supplied as Supplementary Material (Table S1)

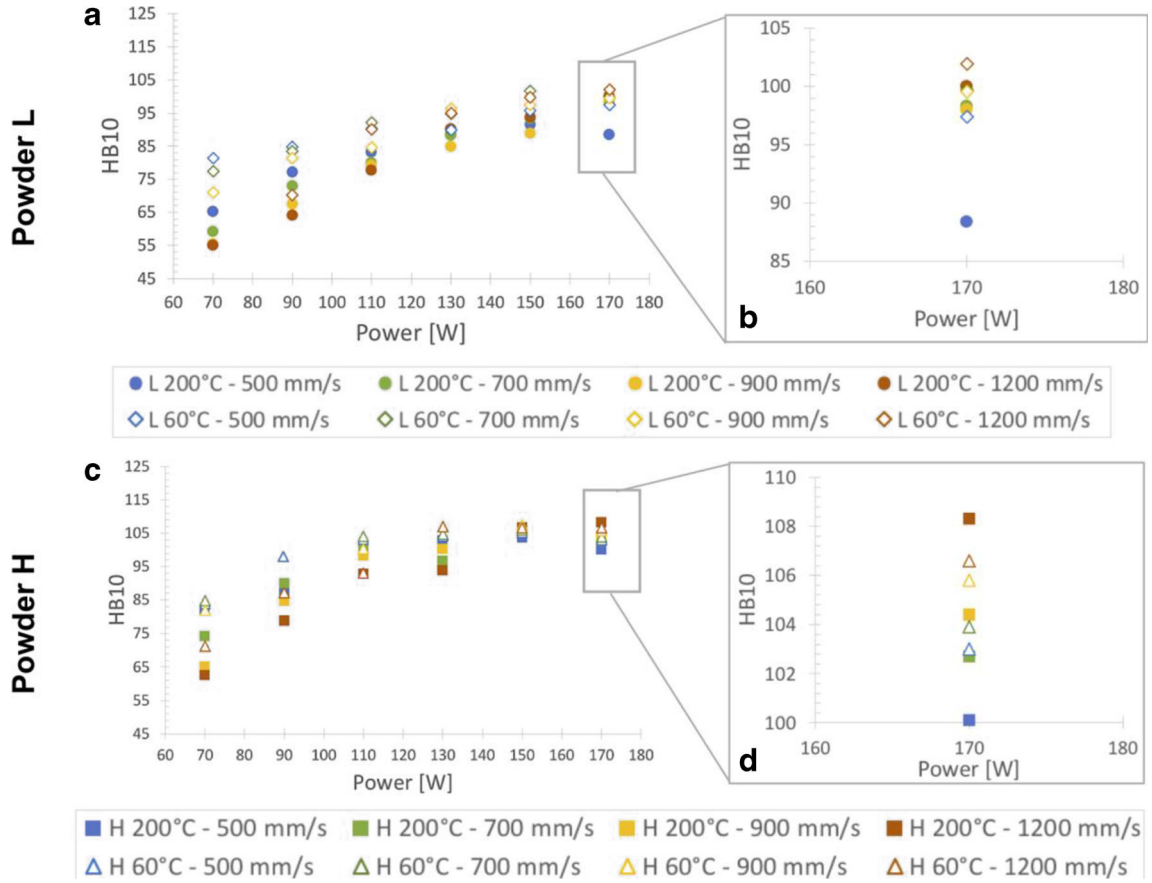

Fig. 7 Results of hardness measurements as a function of laser power and scanning velocities. (a) Samples produced with powder L. (c) Samples produced with powder H. (b, d) Details on samples produced with higher power for powders L and H, respectively. Numerical data are supplied as Supplementary Material (Table S1)

with very low level of oxygen [35]. Thus, in order to successfully consolidate subsequent layers, it is necessary to break the oxide film by operating with high laser power. Furthermore, it has to be taken into consideration that, due to the low absorptivity of aluminum, most of the irradiance of the laser beam is reflected [4], but the efficiency of the process can be improved by exploiting the multiple scattering phenomena occurring among powder particles [36]. Multiple scattering is promoted by spherical powders and, indeed, samples obtained with powder H, being more spherical than powder L, always exhibited higher density, even for values of laser power lower than 110 W, at which powder L exhibited the poorest density. As a consequence, it can be assumed that elongated particles, which are more numerous in powder L, negatively affected the multiple scattering between particles. In addition, the greater flowability of powder H with respect to powder L (Table 2), that is strongly related with the sphericity of particles [22], has likely promoted the spreading of an even and compacted layer during the process. Finally, even though it is not possible to quantify the packing of powders from particle analysis and axis major distribution (Fig. 3), a wide size distribution of spherical powders (as in the case of powder H) generally promotes packaging and increase density of final samples. This consideration agrees with the results obtained in relation to the higher density of the samples realized from powder H, compared with those printed with L.

The influence of scanning velocity is evident in case of powder H (Fig. 6(c, d)) where, for a given laser power, the lowest scanning velocity resulted in samples with maximum density. As already reported in the literature [37, 38], spattering and denudation phenomena can be responsible for the formation of porosities and they are strongly related to laser power and scanning velocity. At high scanning velocities, the two phenomena are accentuated; therefore, it is probable that, for a given laser power, samples processed with the highest scanning velocity had a major content of porosities. Samples obtained from powder L, instead, were more influenced by powder pre-treatment than scanning velocity. As reported in Fig. 6 (a) and (b), the low-temperature pre-treatment maximized density and minimized the contribution ascribable to the scanning velocity; this results are quite evident by focusing on the samples processed at 170 W. More generally, in terms of density, all H and L samples benefited from the powder heat treatment carried out at 60 °C. As mentioned before, powders treated at 200 °C exhibited Al_2O_3, possibly an oxide layer on the powder surface. Thus, in order to melt

Table 5 Chemical composition, measured by GD-OES, of samples produced with the highest volume energy density (P = 170 W, v = 500 mm/s, E = 242.9 J mm^{-3}) considering both powders and pre-treatment conditions

Powder	Pre-treatment	Element (wt.%)					
		Al	Si	Mg	Ti	Fe	Zn
L	60 °C × 3 h	92.445	6.842	0.429	0.103	0.071	0.072
L	200 °C × 1 h	92.236	6.902	0.410	0.108	0.099	0.083
H	60 °C × 3 h	92.397	6.687	0.565	0.150	0.085	0.069
H	200 °C × 1 h	92.356	6.795	0.571	0.123	0.049	0.066

the powder particles, higher power is necessary, with respect to the powder dried at 60 °C, where the oxide layer is not present.

The HB10 hardness of the samples as a function of laser power, for both powders and pre-treatments, is reported in Fig. 7. By increasing the power, the hardness increases, for both powders H and L, as showed by Fig. 7 (a) and (c). The lowest hardness measured was approx. 50–60 HB10 in case of low-density samples while, for samples with the highest density, a maximum of approx. 103 and 108 HB10 were assessed for powders L and H, respectively (Fig. 7(b, d)). The conventional A357 cast alloy reaches the value of up to 100 HB only after the T6 heat treatment [39]; in the present study, instead, the hardness was measured in the as-built samples, within 12 h from the end of the process. Therefore, the SLM process itself succeeded, in the reason of the fine resulting microstructure [6], in obtaining a hardness comparable and even higher than the conventional heat-treated alloy. The low-temperature pre-treatment resulted in samples with greater hardness than the corresponding ones obtained with powders exposed at the high temperature. These results are highlighted by the details in Fig. 7 (b) and (d) for the samples with superior density.

The chemical composition of the SLM samples was evaluated with GD-OES, in case of samples processed with the highest energy density (Table 5). It is well known [5] that high-energy densities might lead to metal vaporization; thus, the control of the chemical composition is necessary. By comparing the results on Table 5 with the requirements for the A357 alloy given by EN 1706 standard, it can be argued that chemical composition of samples obtained with powder H complies with the standard. On the other hand, the Mg content of powder L samples is slightly lower than the one required for the A357 alloy.

The phase composition of selected SLM samples is reported in Fig. 8, where representative samples processed with a constant scanning speed of 900 mm/s and a power of 70 and 150 W are compared, for powders L and H pre-treated at 200 °C.

The only phases detected are Al and Si, so, the Al_2O_3 phase that was observed in the pre-treated powder was not present in the samples. By operating at the highest laser power (170 W), it was possible to obtain a density close to 98% in the case of powder L and over 99% in the case of powder H (being 2.68 g/cm^3 as the reference value for a A357 cast alloy [39]). Nevertheless, by observing the cross-sections of the samples processed at 170 W, few defects could be recognized. Thus, the measurement of the total area occupied by porosities was performed via image analysis, and results are reported in Table 6. The percentage of porosity detected on the cross-section is higher in the case of samples produce with powder L, confirming the results of the density measurement. In addition, results showed that samples with the lowest content of porosity are the ones processed with the highest energy

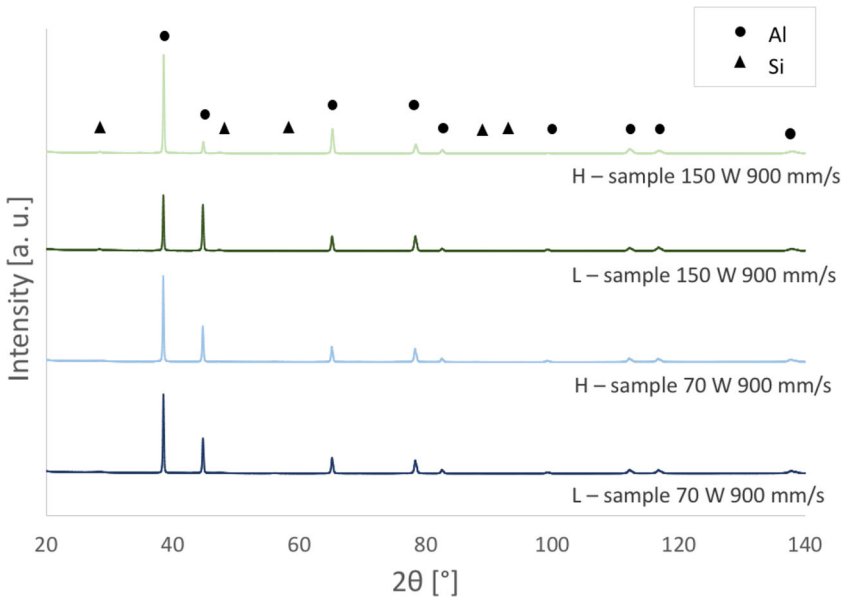

Fig. 8 XRD patterns for samples produced with powders L and H (pre-treated at 200 °C for 1 h) with a scanning velocity of 900 mm/s, in the as-built conditions

Table 6 Results of image analysis performed on cross-sections of SLM samples

Sample	Powder pre-treatment	Powder	Porosity on cross-section (%)	Presence of spatters in the inspected areas (%)	Mean spatter diameter (μm)
170 W–500 mm/s	60° × 3 h	L	1.75	73.3	399 ± 112
		H	0.90	20.0	427 ± 75
170 W–500 mm/s	200 °C × 1 h	L	4.97	66.7	424 ± 112
		H	1.07	40.0	382 ± 98
170 W–1200 mm/s	60° × 3 h	L	2.05	80.0	247 ± 105
		H	2.30	40.0	382 ± 98
170 W–1200 mm/s	200 °C × 1 h	L	3.72	86.7	249 ± 121
		H	2.61	46.7	290 ± 50

density (170 W, 500 mm/s) and adopting the 60 °C heat treatment for powders. However, densities obtained via image analysis are lower than those measured following the Archimedes principle, so, a deeper investigation was carried out by comparing morphological and microstructural features, as reported in Fig. 9.

On the cross-section of samples, large material discontinuities, with dimensions greater than 200 μm, were found, as shown in Fig. 9 (a) and (c). These discontinuities consisted of a round area with a coarser microstructure with respect to the regular microstructure that surrounded the defect, with a cavity lying beneath. It is possible that these large cavities were filled with un-melted powder particles that have been released during the metallographic preparation, thus explaining why density measured by Archimedes principle was overestimated. The round area with a coarse microstructure can be related to the spattering phenomena. As already reported by other researchers [40], who investigated morphological aspects of A357 processed by SLM, spattering, balling, and un-melted powder particles can be found on the surfaces, and un-melted particles and spatters can be distinguished by their microstructure since cooling rates of powders are higher than spatters. In the present study, the majority of powder particles have been proved to be smaller than 60 μm, so it is unlikely that these defects might be related to un-melted particles. In their work [40], indeed, they showed spatters with dimension greater than 200 μm with consistent gas porosity content. With the aim to correlate the defects observed on cross-sections with spatters generation, morphological and microstructural features were compared.

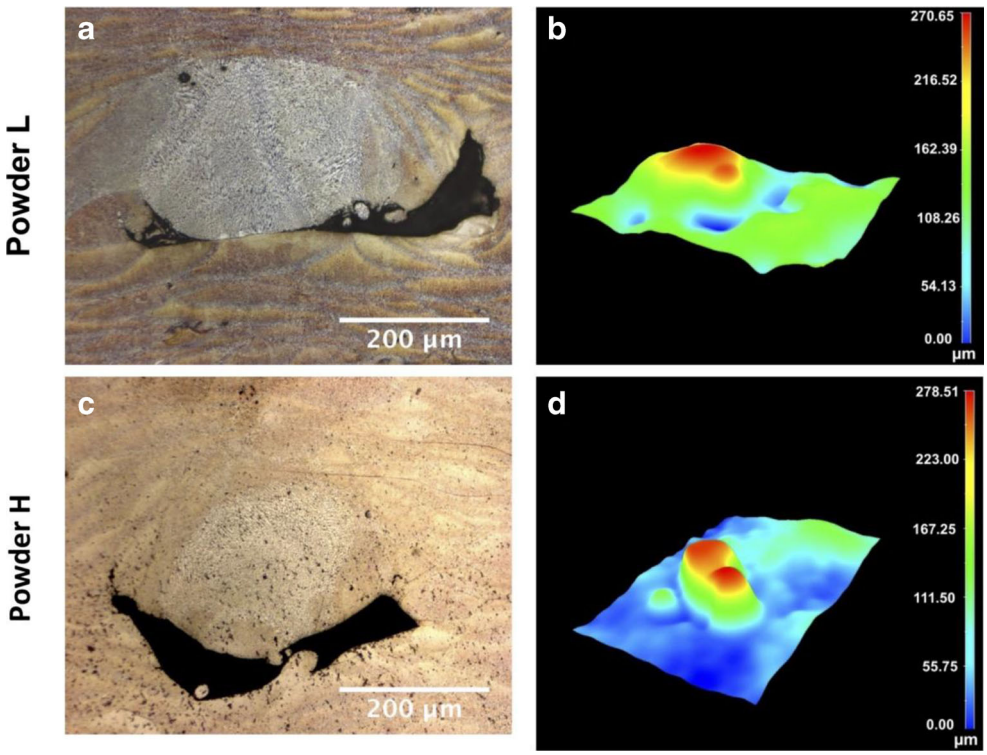

Fig. 9 Results of spatter analysis. (a, c) Optical micrograph of sample cross-section showing a spatter defect for powders L and H, respectively. (b, d) 3D maps of top surfaces of a representative sample for powders L and H, respectively

As regards morphological features, 3D maps of samples' top surfaces were acquired with the 3D digital microscope, as shown in Fig. 9 (b) and (d) for samples processed with a laser power of 170 W and a scanning velocity of 1200 mm/s. Top surfaces were chosen for the analysis since they represent the last processed layer. 3D maps revealed the presence of large spatters on the surfaces with a maximum height of about 270 μm. On the cross-sections, a fixed number of zones were investigated on each sample and for every zone, the presence, or the absence, of the defect was recorded. So, the percentage of spatters identified on the cross-section was evaluated. Furthermore, when a defect was detected, it was measured via image analysis. The results of spatters analysis, also reported in Table 6, demonstrated that a larger extent of such defects was found on samples obtained with powder L than powder H, by a factor of about two. In addition, by comparing the dimensions measured by image analysis with the morphological investigation in Fig. 9 (b) and (d), spatters were positively related to the microstructural defects detected on cross-sections. Spatters are generated during the SLM process and they consist of molten material ejected by the melt pool, then, once solidified, landed on the layer being processed [41, 37]. It can be argued that, since dimensions of spatters are considerably greater than layer thickness and powder particles, they can negatively affect the deposition and the melting of the subsequent layer, as illustrated by Wang et al. [40]; therefore, they can generate microstructural defects. It is worth noting that, both in the case of powders L and H, by increasing the scanning velocity, the amount of spatter defects on cross-section increased accordingly, but their dimension decreased.

Spatter defects were finally analyzed with the aid of SEM-EDS: as disclosed in Fig. 10, spatter defects had high content of spherical gas porosities with dimension lower than 10 μm. In the large cavity underlying the spatter, melted and semi-melted material can be found and the EDS analysis evidenced the presence of elevated concentrations of oxygen in the cavity (spectra 2, 3, 4) with respect to the reference material (spectrum 1).

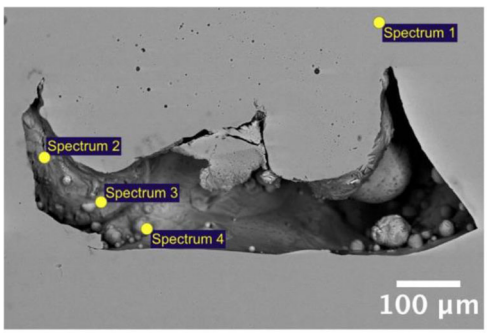

	Element (wt.%)			
	Al	Si	Mg	O
Spectrum 1	90.98	7.38	0.34	1.30
Spectrum 2	60.49	3.21	1.94	34.36
Spectrum 3	78.84	5.37	0.00	15.79
Spectrum 3	82.27	7.10	0.37	10.26

Fig. 10 Results of SEM-EDS analysis performed on a spatter defect detected on sample cross-section

4 Conclusions

Density, hardness and microstructural defects of A357 samples produced by SLM have been analyzed with regard to the feedstock material. Experiments have been carried out with the aim of investigating the effect of the powder conditions in terms of size, morphology, and pre-treatment on the properties of the final components. Based on the outcomes of the present work, the following conclusions can be drawn by separately discussing the influence of the different factors involved in the study.

From powder morphology point of view:

1. For the same process parameters, the powder with particles more spherical than elongated (as powder H) allowed to obtain samples with the highest densities, probably by the reason of the enhanced flowability of the powder.
2. Spherical powders reduced the spattering phenomenon and, consequently, the presence of microstructural defects decreased.

The comparison between results obtained with or without pre-treatment of the powder is even more relevant:

1. As-received powders had a greater number of particles with a diameter ≤ 15 μm compared with the pre-treated ones. Heat treatment of powders probably promoted the aggregation of smaller particles.
2. Pre-treatment did not directly affect the morphology of the powders, but in the case of the powder with the highest amount of very small particles (≤ 10 μm), the percentage of particles with aspect ratio of 1/1.1 decreased with pre-treatment. As mentioned above, this result is probably due to the aggregation phenomena that facilitated the smaller powders to become satellites of the larger ones.
3. XRD analyses evidenced the Al_2O_3 phase both in the as-received powder and pre-treated at 200 °C. On the contrary, powders pre-treated at 60 °C did not exhibit the presence of aluminum oxide.
4. Powder pre-treated at 60 °C resulted in samples with higher density and hardness if compared with the analog ones obtained from powder pre-treated at 200 °C.
5. For the powder with the highest amount of spherical particles, the presence of spatter defects on samples cross-section was twice in the case of pre-treatment at 200 °C compared with the 60 °C one.

Finally, with regard to the process parameters, it is possible to state the following:

1. High-energy density was necessary to reduce porosity.
2. In case of high-energy density, it was also possible to obtain the greatest hardness values. Among the samples with greater hardness, however, the highest values were obtained for the maximum laser scanning speed, probably as a consequence of the different cooling rate.
3. High scanning speeds promoted the formation of spattering, identified by the presence of large microstructural discontinuities; however, the average dimension of such discontinuities was greater in the case of low scanning speed.

Acknowledgments The authors would like to thank Dr. Iuri Boromei at the University of Bologna for his precious contribution in SEM-EDS and XRD analyses.

Compliance with ethical standards

Conflict of interest The authors declare that they have no conflict of interest.

References

1. Mishurova T, Artzt K, Haubrich J, Requena G, Brunoa G (2019) New aspects about the search for the most relevant parameters optimizing SLM materials. Addit Manuf 25:325–334. https://doi.org/10.1016/j.addma.2018.11.023
2. Khorasani AM, Gibson I, Awan US, Ghaderi A (2019) The effect of SLM process parameters on density, hardness, tensile strength and surface quality of Ti-6Al-4V. Addit Manuf 25:176–186. https://doi.org/10.1016/j.addma.2018.09.002
3. Liverani E, Toschi S, Ceschini L, Fortunato A (2017) Effect of selective laser melting (SLM) process parameters on microstructure and mechanical properties of 316L austenitic stainless steel. J Mater Process Technol 249:255–263. https://doi.org/10.1016/j.jmatprotec.2017.05.042
4. Galy C, Le Guen E, Lacoste E, Arvieu C (2018) Main defects observed in aluminum alloy parts produced by SLM: from causes to consequences. Addit Manuf 22:166–175. https://doi.org/10.1016/j.addma.2018.05.005
5. Collins PC, Brice DA, Samimi P, Ghamarian I, Fraser HL (2016) Microstructural control of additively manufactured metallic materials. Annu Rev Mater Res 46:63–91. https://doi.org/10.1146/annurev-matsci-070115-031816
6. Sames WJ, List FA, Pannala S, Dehoff RR, Babu SS (2016) The metallurgy and processing science of metal additive manufacturing. Int Mater Rev 61(5):315–360. https://doi.org/10.1080/09506608.2015.1116649
7. Bartlett JL, Li X (2019) An overview of residual stresses in metal powder bed fusion. Addit Manuf 27:131–149. https://doi.org/10.1016/j.addma.2019.02.020
8. Parry LA, Ashcroft IA, Wildman RD (2019) Geometrical effects on residual stress in selective laser melting. Addit Manuf 25:166–175. https://doi.org/10.1016/j.addma.2018.09.026
9. Yamaguchi H, Fergani O, Wua P (2017) Modification using magnetic field-assisted finishing of the surface roughness and residual stress of additively manufactured components. CIRP Ann Manuf Technol 66:305–308. https://doi.org/10.1016/j.cirp.2017.04.084
10. Kaynaka, Y., Kitay, O., The effect of post-processing operations on surface characteristics of 316L stainless steel produced by selective laser melting, https://doi.org/10.1016/j.addma.2018.12.021.
11. Fortunato A, Lulaj A, Melkote S, Liverani E, Ascari A, Umbrello D (2018) Milling of maraging steel components produced by selective laser melting. Int J Adv Manuf Technol 94:1895–1902. https://doi.org/10.1007/s00170-017-0922-9
12. Anderson IE, White EMH, Dehoff R (2018) Feedstock powder processing research needs for additive manufacturing development. Curr Opinion Solid State Mater Sci 22:8–15. https://doi.org/10.1016/j.cossms.2018.01.002
13. Tan JH, Wong WLE, Dalgarno KW (2017) An overview of powder granulometry on feedstock and part performance in the selective laser melting process. Addit Manuf 18:228–255. https://doi.org/10.1016/j.addma.2017.10.011
14. Pleassa C, Jothia S (2018) Influence of powder characteristics and additive manufacturing process parameters on the microstructure and mechanical behaviour of Inconel 625 fabricated by selective laser melting. Addit Manuf 24:419–431. https://doi.org/10.1016/j.addma.2018.09.023
15. Nguyen QB, Nai MLS, Zhu Z, Sun C-N, Wei J, Zhou W (2017) Characteristics of Inconel powders for powder-bed additive manufacturing. Engineering 3:695–700. https://doi.org/10.1016/J.ENG.2017.05.012
16. Spierings, A.,B., Levy, G., Comparison of density of stainless steel 316L parts produced with selective laser melting using different powder grades, Annual International SFF Symposium, Austin, University of Texas, (2009) 342–353.
17. Spierings AB, Herres N, Levy G (2011) Influence of the particle size distribution on surface quality and mechanical properties in AM steel parts. Rapid Prototyp J 17(3):195–202. https://doi.org/10.1108/13552541111124770
18. Karapatis, N.P., A sub-process approach of selective laser sintering. 2002, Ecole Polytechnique fédérale de Lausanne EPFL: Lausanne, https://doi.org/10.5075/epfl-thesis-2506.
19. Baitimerov R, Lykov P, Zherebtsov D, Radionova L, Shultc A, Prashanth KG (2018) Influence of powder characteristics on processability of AlSi12 alloy fabricated by selective laser melting. Materials 11(5):742. https://doi.org/10.3390/ma11050742
20. Muñiz-Lerma JA, Nommeots-Nomm A, Waters KE, Brochu M (2018) A Comprehensive approach to powder feedstock characterization for powder bed fusion additive manufacturing: a case study on AlSi7Mg. Materials 11:2386. https://doi.org/10.3390/ma11122386
21. Hebert RJ (2016) Viewpoint: metallurgical aspects of powder bed metal additive manufacturing. J Mater Sci 51:1165–1175. https://doi.org/10.1007/s10853-015-9479-x
22. Vock S, Klöden B, Kirchner A, Weißgärber T, Kieback B (2019) Powders for powder bed fusion: a review. Progress in Additive Manufacturing:1–15. https://doi.org/10.1007/s40964-019-00078-6
23. Asgaria H, Baxtera C, Hosseinkhani K, Mohammadi M (2017) On microstructure and mechanical properties of additively manufactured AlSi10Mg_200C using recycled powder. Mater Sci Eng A 707:148–158. https://doi.org/10.1016/j.msea.2017.09.041
24. Clayton J, Millington-Smith D, Armstrong B (2015) The application of powder rheology in additive manufacturing. J Min Met Mater Soc 67:544–548. https://doi.org/10.1007/s11837-015-1293-z
25. Li XP, O'Donnell KM, Sercombe TB (2016) Selective laser melting of Al-12Si alloy: enhanced densification via powder drying. Addit Manuf 10:10–14. https://doi.org/10.1016/j.addma.2016.01.003
26. Cayless RBC (1990) Alloy and temper designation systems for aluminum and aluminum alloys, properties and selection: nonferrous alloys and special-purpose materials, ASM Handbook. https://doi.org/10.31399/asm.hb.v02.9781627081627

27. Carpenter Technology Corporation, Available: www.carpenteradditive.com
28. Rueden CT, Schindelin J, Hiner MC, DeZonia BE, Walte AE, Arena ET, Eliceiri KW (2017) ImageJ2: ImageJ for the next generation of scientific image data. BMC Bioinformatics 18(1):529. https://doi.org/10.1186/s12859-017-1934-z
29. Vander Voort, G.F., ASM Handbook Volume 9 - Metallography and microstructures, ASM International, 2004.
30. Fiorese E, Bonollo F, Timelli G, Arnberg L, Gariboldi E (2015) New classification of defects and imperfections for aluminum alloy castings. Int J Met 9(1):55–66. https://doi.org/10.1007/BF03355602
31. Walton OR Review of adhesion fundamentals for micron scale particles. Kona Powder Part J 26(26):129–141. https://doi.org/10.14356/kona.2008012
32. Yablokova G, Speirs M, Van Humbeeck J, Kruth J-P, Schrooten J, Cloots R, Boschini F, Lumay G, Luyten J (2015) Rheological behavior of β-Ti and NiTi powders produced by atomization for SLM production of open porous orthopedic implants. Powder Technol 283:199–209. https://doi.org/10.1016/j.powtec.2015.05.015
33. Lamouri S, Hamidouche M, Bouaouadja N, Belhouchet H, Garnier V, Fantozzi G, Trelkat JF (2016) Control of the γ-alumina to α -alumina phase transformation for an optimized alumina densification. Boletín de la Societad Española de Cerámica y Vidrio 6(56):47–54. https://doi.org/10.1016/j.bsecv.2016.10.001
34. Hryha E, Shvab R, Gruber H, Leicht A, Nyborg L (2018) Surface oxide state on metal powder and its changes during additive manufacturing: an overview. La Metallurgia Italiana 3:34–39
35. Louvis E, Fox P, Sutcliffe CJ (2011) Selective laser melting of aluminium components. J Mater Process Technol 211(2):275–284. https://doi.org/10.1016/j.jmatprotec.2010.09.019
36. Boley CD, Khairallah SA, Rubenchik AM (2015) Calculation of laser absorption by metal powders in additive manufacturing. Appl Opt 54(9):2477–2482. https://doi.org/10.1364/AO.54.002477
37. Bidare P, Bitharas I, Ward RM, Attallah MM, Moore AJ (2018) Fluid and particle dynamics in laser powder bed fusion. Acta Mater 142:107–120. https://doi.org/10.1016/j.actamat.2017.09.051
38. Matthews MJ, Guss G, Khairallah SA, Rubenchik AM, Depond PJ, King WE (2016) Denudation of metal powder layers in laser powder bed fusion processes. Acta Mater 114:33–42. https://doi.org/10.1016/j.actamat.2016.05.017
39. Sigworth G (2018) Aluminum casting alloys and casting processes, Aluminum Science and Technology, ASM Handbook, https://doi.org/10.31399/asm.hb.v02a.9781627082075
40. Nasab MH, Gastaldi D, Lecis NF, Vedani M (2018) On morphological surface features of the parts printed by selective laser melting (SLM). Addit Manuf 24:373–377. https://doi.org/10.1016/j.addma.2018.10.011
41. Wang D, Wu S, Fu F, Mai S, Yang Y, Liu Y, Song C (2017) Mechanisms and characteristics of spatter generation in SLM processing and its effect on the properties. Mater Des 117:121–130. https://doi.org/10.1016/j.matdes.2016.12.060